Experimental sensitivity analysis via a secondary heat source in an oscillating thermoacoustic system

$SAGE

Nicholas P Jamieson[1], Georgios Rigas[2], and Matthew P Juniper[1]

Abstract

In this paper, we report the results of an experimental sensitivity analysis on a vertical electrically-heated Rijke tube. We examine the stability characteristics of the system due to the introduction of a secondary heat source. The experimental sensitivity analysis is quantified by measuring the shift in linear growth and decay rate as well as the shift in the linear frequency during periods of growth and decay of thermoacoustic oscillations. Linear growth and decay rate measurements agree qualitatively well with the theoretical predictions from adjoint-based methods of Magri & Juniper (*J. Fluid Mech.*, vol. 719, 2013, pp. 183-202). A discrepancy in the linear frequency measurements highlight deficiencies in the model used for those predictions and shows that the experimental measurement of sensitivities is a stringent test of any thermoacoustic model. The findings suggest that adjoint-based methods are, in principle, capable of providing industry with a cheap and efficient tool for developing optimal control strategies for more complex thermoacoustic systems.

Introduction

In many combustion systems, there exist high-amplitude pressure oscillations whose frequency ranges are close to those of the natural acoustic modes of the system. These are known as thermoacoustic oscillations and arise from the feedback loop between acoustic waves and unsteady heat release if the latter occurs sufficiently in phase with unsteady pressure. The oscillations can threaten the operability and reliability of combustion systems by increasing the risks of thrust oscillations, mechanical vibration, and excessive thermal and mechanical loading, resulting in decreased efficiency and ultimately system failure (Lieuwen and Yang 2005). More recently, the suppression of thermoacoustic oscillations has become an important consideration for the gas turbine industry. Stricter legislation regarding the emission of NO_x has led engine manufacturers to operate under a lean and premixed regime. This shift in gas turbine operation often leads to the excitation of thermoacoustic oscillations due to equivalence ratio fluctuations (Lieuwen and Zinn 1998).

In this paper, we investigate the control of an electrically-heated Rijke tube via a secondary heat source with a constant power input. The secondary heat source is traversed through a range of axial locations inside the tube. The main novelty is that we extend the work of Rigas et al. (2016) to carefully measure and compare experimental results with theoretical predictions from adjoint based sensitivity analysis.

The Rijke tube and control

The Rijke tube, first proposed by Rijke (1859), is a simple configuration through which thermoacoustic phenomena can be studied (Raun et al. 1993). To a reasonable approximation, the pressure fluctuation at the open ends of the Rijke tube is zero. Therefore the fundamental mode has a pressure node at both ends and an antinode in the middle. The acoustic velocity has a node at the centre and an antinode at each end. During the compression phase of the acoustic cycle, the acoustic velocity is directed towards the centre of the tube, causing the pressure in the tube to increase. When the heater is placed in the upstream half of the tube, the acoustic velocity and the mean velocity are in the same direction during the compression phase. This means that the air speed around the heater, and therefore the heat transfer, are greater than average during the compression phase. Crucially, there is also a time delay (Lighthill 1954) between the velocity at the heater and the subsequent heat release. These two features mean that, over an acoustic cycle, more heat release occurs during moments of higher pressure than occurs during moments of lower pressure. This causes more mechanical work to be done by the gas expanding during the expansion phase than was required to compress it during the compression phase (Rayleigh 1878). This causes the amplitude of acoustic oscillations to grow until the extra work is dissipated through acoustic radiation

[1]Department of Engineering, University of Cambridge, Trumpington Street, Cambridge CB2 1PZ, UK
[2]Department of Mechanical and Civil Engineering, California Institute of Technology, Pasadena, CA 91125, USA

Corresponding author:
Nicholas P Jamieson, Department of Engineering, University of Cambridge, Trumpington Street, Cambridge CB2 1PZ, UK.
Email: npj24@cam.ac.uk

and viscous/thermal losses, at which point a limit cycle is reached.

The control methods used to suppress thermoacoustic oscillations can be divided into two categories: passive and active (McManus et al. 1993; Candel 2002; Dowling and Morgans 2005). Passive control can be achieved by modifying the design or adding devices, such as Helmholtz resonators. A famous example of this is demonstrated by the use of baffles in the development for the F1 engine of the Saturn V rocket used in the Apollo space missions. During the development of these engines, pressure oscillations of approximately 100% of the mean combustor pressure occurred at a frequency between 200 and 500 Hz. In this instance, approximately 2000 full-scale tests were conducted to mitigate these oscillations (Culick 1988).

Active control of thermoacoustic oscillations can be achieved via either open-loop control or closed-loop feedback control. Some of the earliest papers to report the open-loop control of thermoacoustic oscillations in a Rijke tube are by Katto and Sajiki (1977) and Sreenivasan et al. (1985). These studies showed that oscillations present in a flame-driven Rijke tube can be suppressed by introducing a control heater downstream of the primary heater at certain positions. Katto and Sajiki (1977) found that when a primary heater is located at $x_p/L = 0.25$, an identical secondary heat source located at $x_c/L = 0.75$ had a stabilising effect on the system. Where x_p and x_c is the position of the primary heater and secondary heat source respectively, and L is the length of the Rijke tube.

Heckl (1988) used a feedback control system consisting of a microphone upstream of the heat source, which produced a signal that is then phase-shifted, amplified and transmitted to a loudspeaker downstream. This feedback loop proved successful in suppressing thermoacoustic oscillations within the Rijke tube. Recent work on the active control of thermoacoustic oscillations is shown in Zhang et al. (2015) and Zhao et al. (2015). In Zhang et al. (2015), a tunable Helmholtz resonator is used to control thermoacoustic oscillations. The Helmholtz resonator is optimised by modifying its throat area in real-time, thus allowing it to suppress thermoacoustic oscillations over a large frequency range. Zhao et al. (2015) employ active open-loop forcing via an electrical heater to suppress thermoacoustic oscillations in a premixed flame-driven Rijke tube. Zhao et al. (2015) found that the optimal location to place the secondary heat source is in the range $0.72 \leq x_c/L \leq 0.75$ for a system with a resonant frequency of 240 Hz. It is also found that in this location range, the resonant sound pressure level could be decreased by 70 dB as the power input to the secondary heat source is increased to 218.2 W.

Sensitivity analysis and adjoint methods in thermoacoustics

Sensitivity analysis typically quantifies (i) the sensitivity of each mode to internal feedback, known here as the feedback sensitivity, achieved by introducing a passive device and, (ii) the sensitivity of each mode to changes in the base state, known here as the base-state sensitivity, achieved by design modifications to the system (Magri and Juniper 2013). Further information can be found in the recent reviews of Sipp et al. (2010), Luchini and Bottaro (2014) and Schmid and Brandt (2014). Historically, sensitivity analysis is performed via the finite difference approach. However, this method is computationally expensive and prone to numerical error. Given these limitations, adjoint methods have been found to offer a more efficient and accurate means of conducting sensitivity analyses. The application of adjoint methods to sensitivity analysis in thermoacoustics has been developed over the past few years (Magri and Juniper 2013, 2014a,b).

The study by Magri and Juniper (2013) is the most relevant because the experimental set-up utilised in this paper consists of a Rijke tube with a gauze heater acting as the acoustically compact heat source. Using adjoint methods, they calculated how the linear growth rate and frequency of thermoacoustic oscillations change when; (i) a passive control device is introduced to the system, and (ii) a secondary heat source with a constant power is introduced to the system. For the passive control case they found that the growth rate of oscillation is most sensitive to a feedback mechanism that is proportional to the velocity and that forces the momentum equation. This type of feedback could be physically implemented in the form of a mesh, which forces the momentum equation in the opposite direction to the velocity by inducing a drag force. Magri and Juniper (2013) also found that the passive device has the largest effect when placed at the ends of the Rijke tube. In the second case, they found as expected that the secondary heat source had a stabilising effect when placed in the top half of the tube, $x_c/L = 0.5$ to 1, and a destabilising effect when placed in the bottom half of the tube, $x_c/L = 0$ to 0.45. The aim of our work in this paper is to experimentally investigate the adjoint-based predictions of Magri and Juniper (2013) for the case of control via a secondary heat source.

A study by Rigas et al. (2016) provided the first comparison of experimental sensitivity analysis with adjoint-based sensitivity analysis in thermoacoustics. Linear growth rates and decay rates were obtained for a range of different primary heater powers and axial locations of a passive drag device, x_c/L. By subtracting the baseline linear growth rate and linear decay rate obtained in absence of a passive drag device from the linear growth rates and decay rates obtained with a passive drag device installed, Rigas et al. (2016) were able to ascertain the sensitivity of the linear growth and decay rate due to the introduction of a passive drag device. The results of the experimental sensitivity analysis were compared to the adjoint-based predictions of Magri and Juniper (2013) (figure 1), finding good qualitative agreement for the growth rate shift, but not the frequency shift. The poor agreement for the frequency shift is because the model used by Magri and Juniper (2013) did not account for the mean shift in flow rate caused by the control device.

Experimental Setup

Experiments were conducted on a 1 m long stainless steel vertical Rijke tube with an internal diameter of 47.4 mm and a wall thickness of 1.7 mm. Two identical heaters were used. The primary heater is attached to two rods and held in place at $x_p/L = 0.25$, the optimal position for exciting thermoacoustic oscillations (Saito 1965). It is powered by
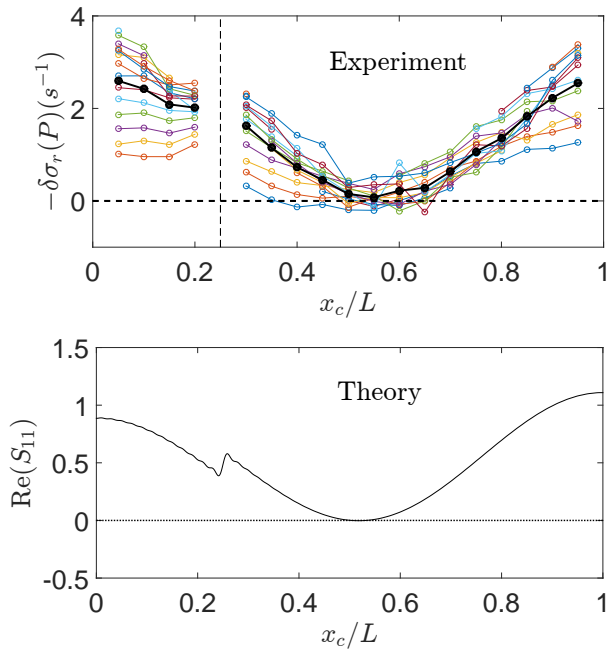
Figure 1. Sensitivity of the growth rate, $\delta\sigma_r$, to a passive drag device placed at position x_c/L. Each experimental curve corresponds to a different primary heater power. Top: experimental results, note that the average sensitivity is also shown (solid lines). Bottom: theoretical predictions of Magri and Juniper (2013), where $Re(S_{11})$ is the shift in growth rate (arbitrary units) due to the introduction of a passive drag device placed at position x_c/L.

a 640 Watt EA Elektro-Automatik EA-PSI 5080-20 A DC programmable power supply. The secondary heat source is used with a constant power input for the experiment detailed in this paper. The secondary heat source is attached to an automated digital height gauge at the top of the Rijke tube, enabling it to be automatically traversed with an accuracy of $\pm\,0.01$ mm.

A Brüel Kjaer condenser type 2619 microphone with a sensitivity of 11.4 mV Pa^{-1} is used to measure pressure fluctuations. The microphone is angled at $45°$ and placed 55 mm from the bottom end of the tube. The raw pressure signal is sampled at 10 kHz, much higher than the anticipated frequencies of the thermoacoustic oscillations, approximately 190 Hz. Data is acquired via a National Instruments BNC-2110 DAQ device using LabVIEW. The setup used is shown in figure 2.
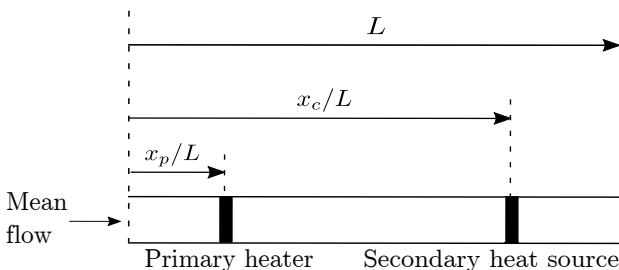

Figure 2. Schematic of experimental setup. In the experiment, a constant power input is given to the secondary heat source.

Control via a secondary heat source

In this section, we investigate the control of an electrically-heated Rijke tube via the introduction of a secondary heat source. The aim of this work is to extend the methods described in Rigas et al. (2016) and carefully compare experimental results with the theoretical predictions of adjoint-based methods.
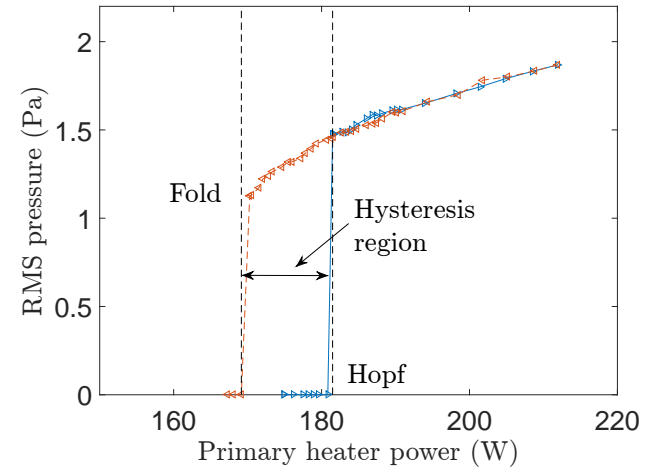

Figure 3. Sub-critical Hopf bifurcation diagram obtained experimentally with no secondary heat source (Rigas et al. 2016).

Methodology

The dynamical system behaviour of the system is characterised by a sub-critical Hopf bifurcation (figure 3). The system can be made to transition from a stable fixed point to a stable limit-cycle if the control parameter, in this case the primary heater power, is increased above the Hopf point. Similarly, the system can be made to transition from a stable limit-cycle to a stable fixed point if the same control parameter is decreased below the fold point. There also exists a hysteresis region between the Hopf and fold points. It is during these periods of growth and decay of thermoacoustic oscillations that we can extract the linear growth and decay rates.

The raw pressure signals that show the thermoacoustic oscillations growing and decaying from a stable fixed point to a stable limit-cycle and vice versa are shown in figure 4a and 4b. The Hilbert transform is then applied to the raw pressure signal to obtain the instantaneous amplitude, $A(t)$, and phase $\phi(t)$ (Schumm et al. 1994) (figure 4c and 4d). A bandpass Butterworth filter is applied to the Hilbert transformed signal leading to a noise-free region of linear growth and decay to be found between two limits. The upper and lower limits were set to ensure that the linear fit is not influenced by nonlinear effects or the noise floor. The linear growth rates, σ_r, and the linear frequencies, σ_i, were obtained by $d(log(A))/dt$ and $d(\phi)/dt$, respectively.

Experiments were performed for a range of operating points (figure 5). The experimental procedure is comprised of three steps: (i) the system is heated up to a steady state with a primary heater power input of ≈ 138 W, (ii) the
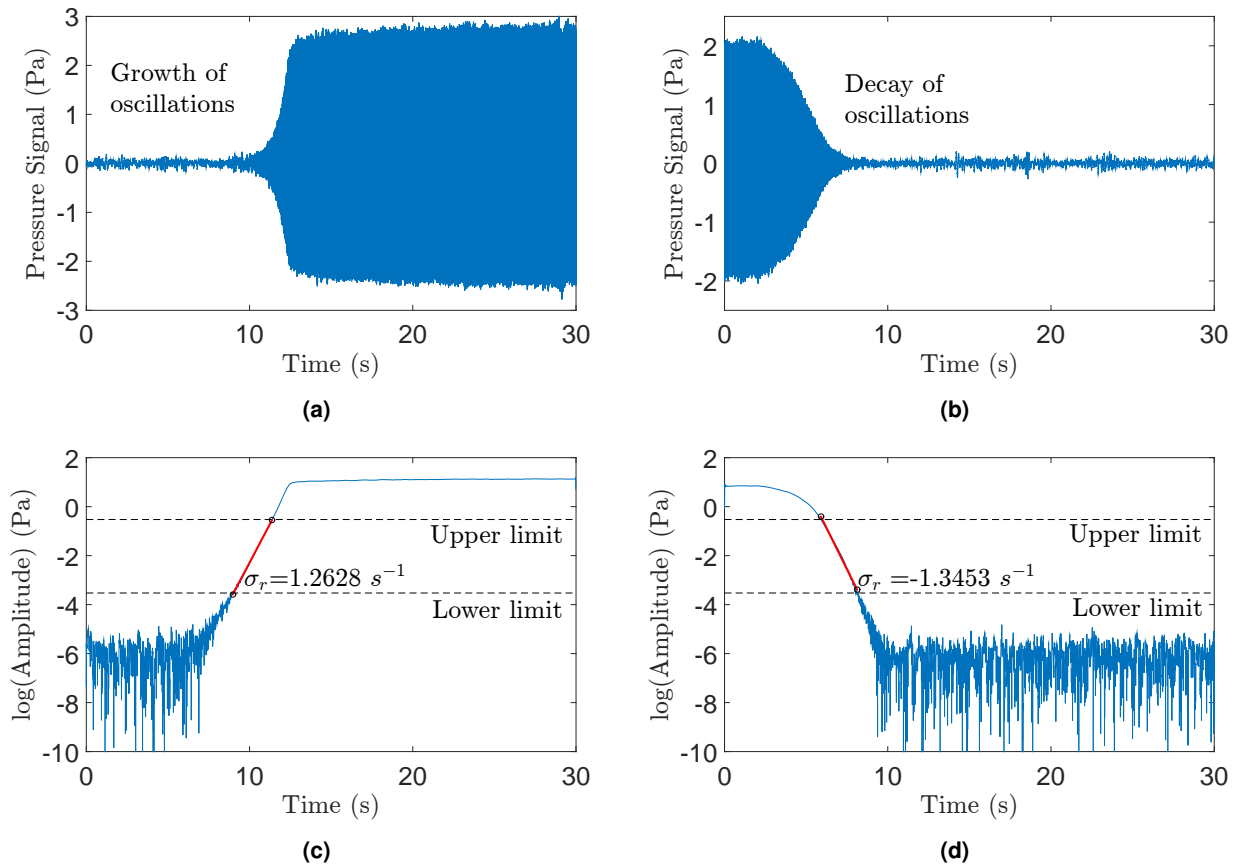
Figure 4. (a) Pressure signal obtained by increasing the primary power input from $P_{Hopf} - 15$ W to $P = 223$ W. Thermoacoustic oscillations grow as the system transitions from a stable fixed point to a stable limit-cycle. (b) Pressure signal obtained by decreasing the primary power input $P_{fold} + 15$ W to $P = 140$ W. Thermoacoustic oscillations decay as the system transitions from a stable limit-cycle to a stable fixed point. (c) Amplitude of the filtered pressure signal obtained using the Hilbert transform. The linear growth rate is shown in red between the lower and upper limits. (d) Amplitude of the filtered pressure signal obtained using the Hilbert transform. The linear decay rate is shown in red between the lower and upper limits. This figure is obtained from Rigas et al. (2016).

power input to the primary heater is then abruptly increased to ≈ 393 W, and the linear growth rate is measured as the system transitioned from a stable fixed point to a stable limit-cycle, and (iii) the power input to the primary heater is then abruptly decreased to ≈ 138 W, and the linear decay rate is measured as the system transitioned from a stable limit-cycle to a stable fixed point. For both heating and cooling, the heater reaches its new steady state within 2 seconds. The air velocity through the tube is around 0.5 ms^{-1}, meaning that a complete flush takes around 2 seconds. The growth and decay rates are measured between 5 and 12 seconds after the heater power is changed, which is after the Rijke tube has reached its new steady state.

For each of the above steps, the secondary heat source is held at a constant power. The secondary heat source is then given a range of predetermined power inputs, seen as the corresponding horizontal-axis power for a given acquisition point 'x' in figure 5, and the same process repeated.

The secondary heat source is traversed from $x_c/L = 0.05$-0.2 and 0.3-0.95 in 0.05 increments. At each examined location, the acquisition process is repeated three times with no power input to the secondary heat source to obtain a baseline growth rate, $\sigma_{0,r,g}$, decay rate, $\sigma_{0,r,d}$, frequency during the period of linear growth, $\sigma_{0,i,g}$, and the frequency during the period of linear decay, $\sigma_{0,i,d}$. The subscript c
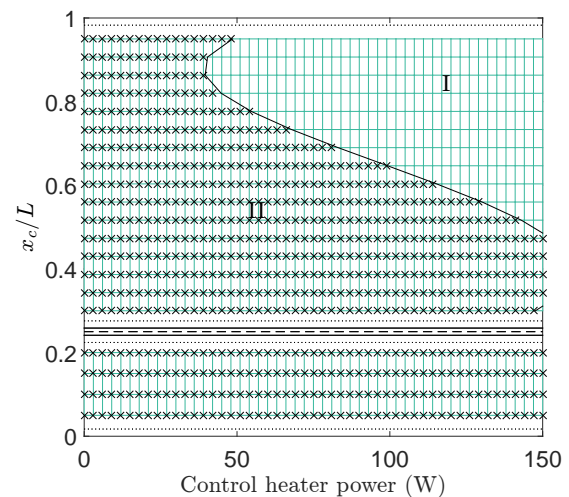

Figure 5. Experimental operating range. 'x' mark a point where a growth rate, decay rate and frequency measurement is acquired. Dashed lines at $x_c/L = 0.25$ indicate the location of the primary heater. The experiment is repeated five times at each data point.

corresponds to the control case (heater on) and the subscript 0 to the baseline case (heater off).
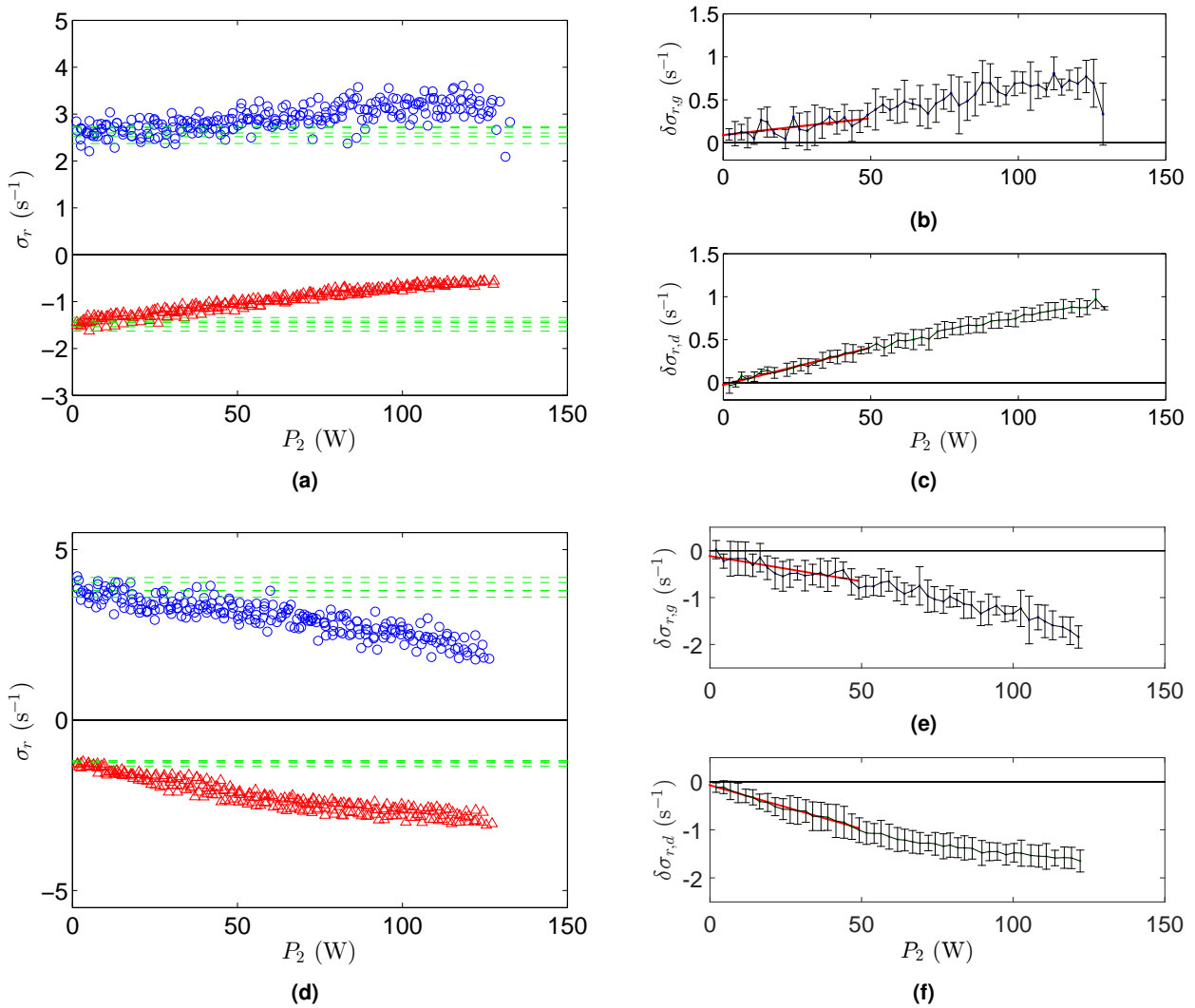
Figure 6. (a) $x_c/L = 0.35$: Growth rates (blue) and decay rates (red) obtained for a range of secondary heat source powers. All baseline runs are shown in the green; (b) $x_c/L = 0.35$: difference between growth rate with the secondary heat source and the baseline growth rate, $\delta\sigma_{r,g}$; (c) $x_c/L = 0.35$: difference between decay rate with the secondary heat source and the baseline decay rate, $\delta\sigma_{r,d}$; (d) $x_c/L = 0.55$: Growth rates (blue) and decay rates (red) obtained for a range of secondary heat source powers. All baseline run is shown in the green; (e) $x_c/L = 0.55$: difference between growth rate with the secondary heat source and the baseline growth rate, $\delta\sigma_{r,g}$; (f) $x_c/L = 0.55$: difference between decay rate with the secondary heat source and the baseline decay rate, $\delta\sigma_{r,d}$.

At axial locations $x_c/L = 0.55$-0.95, the range of examined secondary heat source powers is reduced. In region I (figure 5), the abrupt step in the primary heater power did not cause the system to transition from a stable fixed point to a stable limit-cycle. This is due to limitations in the power supply used to power the primary heater to overcome the stabilising effect of the secondary heat source. Therefore, we were only able to conduct the experiment in region II.

The novelty in our experimental setup is that the entire process is automated. We were able to acquire each data point exhibited in figure 5 in approximately 42 hours of testing. To ensure repeatability of results, the experiment is repeated five times such that a detailed uncertainty analysis could be performed.

The shift in linear growth rate and decay rate defined in the theoretical analysis of Magri and Juniper (2013) is obtained

experimentally as

$$\delta\sigma_{r,g}(P_2, P_{p,1}, P_{p,2}, x_c) = \sigma_{c,r,g}(P_2, P_{p,1}, P_{p,2}, x_c)... \\ -\sigma_{0,r,g}(x_c, P_{p,1}, P_{p,2}). \quad (1)$$

$$\delta\sigma_{r,d}(P_2, P_{p,1}, P_{p,2}, x_c) = \sigma_{c,r,d}(P_2, P_{p,1}, P_{p,2}, x_c)... \\ -\sigma_{0,r,d}(x_c, P_{p,1}, P_{p,2}). \quad (2)$$

where P_2 is the power to the secondary heat source, $P_{p,2}$ is the power to the primary heater when the system is at a stable limit-cycle, and $P_{p,1}$ is the power to the primary heater when the system is at a stable fixed point.

Measurement of linear growth and decay rates

The growth and decay rates were measured experimentally for a range of secondary heat source powers, P_2, and secondary heat source axial locations, x_c/L. It is recalled

that growth rates at $P_2 = 0$ W vary with x_c/L (Rigas et al. 2016).

To determine the shift in growth rate and decay rate due to the presence of a secondary heat source the data obtained at each location were processed in the same way. For brevity, the data for only $x_c/L = 0.35$ and $x_c/L = 0.55$ are presented here (figure 6).

Figure 6a shows the growth rates (blue circles) and decay rates (red triangles) obtained over the course of the five repeated experiments at $x_c/L = 0.35$. The baseline growth rates and baseline decay rates are plotted in the dashed green lines. Each green line corresponds to a baseline obtained for data taken on a particular day. Figure 6d shows the same but for $x_c/L = 0.55$. The reason the baseline measurement changes between days is most likely due to ambient temperature changes in the laboratory.

Figure 6b shows the difference between the growth rate obtained with the secondary heat source, $\sigma_{c,r,g}$, and the baseline growth rate, $\sigma_{0,r,g}$, at $x_c/L = 0.35$. The data obtained over the five experiments were averaged and the mean is plotted. To extract the shift in linear growth rate, a least-squares regression fitting has been performed between 0 W and 50 W, the region where the shift in growth rate is deemed to be linear. At high amplitudes above the threshold of 50 W we found that the trend became nonlinear. Figure 6c shows the difference between the decay rate obtained with the secondary heat source, $\sigma_{c,r,d}$, and the baseline decay rate, $\sigma_{0,r,d}$. Figure 6e and 6f show the same for $x_c/L = 0.55$. Error bars are presented for each data point in figure 6b, 6c, 6e and 6f. Uncertainties, with a 95 % confidence interval, are presented in figure 6. The uncertainty analysis is discussed in Appendix A.

It can be seen that the gradient of the data in figure 6a, 6b and 6c is positive, whilst the gradient of the data in figure 6d, 6e and 6f is negative. This demonstrates that the presence of the secondary heat source has a destabilising effect in the bottom half of the tube, $x_c/L = 0.35$, and a stabilising effect when placed in the top half of the tube, $x_c/L = 0.55$.

Measurement of frequency during linear growth and decay of oscillations

The frequencies during the linear growth and decay of the thermoacoustic oscillations were obtained for a variety of secondary heat source powers, P_2, and secondary heat source axial locations. Data were obtained over the same operating range as for the growth and decay rate measurements.

To determine the shift in the frequency during the period of linear growth and decay of the oscillations due to a secondary heat source, the data is processed at each axial location in the same way. For brevity, only the data for $x_c/L = 0.35$ and $x_c/L = 0.55$ are presented here (figure 7).

Figure 7a shows the frequency during the linear growth of the oscillations (blue circles) and the frequency during the linear decay of the oscillations (red triangles). The baseline frequencies exhibited during these periods are denoted by the green dashed line. Each baseline frequency measurement corresponds to the data taken on a particular day.

Figure 7b shows the difference between the frequency during the linear growth of the oscillations obtained with a secondary heat source on, $\sigma_{c,i,g}$, and the baseline frequency

during the linear growth of oscillations, $\sigma_{0,i,g}$. The data obtained over the five experiments is averaged and the mean is plotted. The shift in frequency during the period of linear growth of oscillations is extracted in the same way as discussed for figure 6b. Figure 7c shows the difference between the frequency during the linear decay of the oscillations obtained with a secondary heat source on, $\sigma_{c,i,d}$, and the baseline frequency during the linear decay of oscillations, $\sigma_{0,i,d}$. The data obtained over the five experiments were averaged and the mean is plotted. Figure 7e and 7f show the same for $x_c/L = 0.55$. Error bars are presented for each data point in figure 7b, 7c, 7e and 7f. Uncertainties, with a 95 % confidence interval, are presented in figure 7. The uncertainty analysis is discussed in Appendix A.

It can be seen that the gradient of the data in each subplot of figure 7 is positive. For the frequency measurements, this is expected as by increasing the secondary heat source power we are always increasing the temperature of the mean flow in the Rijke tube. As the flow temperature increases, the local speed of sound will also increase resulting in a positive increase in frequency of oscillation (Rigas et al. 2016). This does not support the predictions of Magri and Juniper (2013) because they do not take into account base flow modifications caused by an increase in mean flow temperature.

Shift in linear growth and decay rate

This section presents the experimental sensitivity analysis results detailing the shift in linear growth and decay rate due to the introduction of a secondary heat source.

Figure 8a and 8b show $\delta\sigma_{r,g}$ and $\delta\sigma_{r,d}$ for $x_c/L = 0.1$, 0.15, 0.35, 0.45, 0.55, 0.75, and 0.85. These points were chosen so that a clear depiction could be obtained of how the gradient of the $\delta\sigma_{r,g}$ and $\delta\sigma_{r,d}$ data varies as the secondary heat source is traversed through a range of axial locations. The coloured patching around the mean $\delta\sigma_{r,g}$ and $\delta\sigma_{r,d}$ represents the uncertainty in the measurement at that axial location. It can be seen that at axial locations $x_c/L = 0.75$ and 0.85, the uncertainty is larger. The reason for this is that we have fewer data points when compared with other axial locations.

Figure 8c presents the experimental sensitivity analysis results for the shift in linear growth rate (blue) and linear decay rate (red) due to the introduction of secondary heat source. We compare the experimental results with the predictions of Magri and Juniper (2013) (figure 8d) and find that they qualitatively compare well. It can be seen in figure 8c that the introduction of a secondary heat source has a destabilising effect when placed between $x_c/L = 0.05$ and $x_c/L = 0.4$. Magri and Juniper (2013) found that this is because when the secondary heat source is placed between $x_c/L = 0.05$ and $x_c/L = 0.4$, the acoustic pressure and unsteady heat-release are sufficiently in phase, making a positive contribution to the growth of oscillation over a cycle. When the secondary heat source is placed between between $x_c/L = 0.45$ and $x_c/L = 0.95$, figure 8c shows that it has a stabilising effect on the system. This is because in this region, the acoustic pressure and unsteady heat-release are out of phase such that they negatively contribute to the growth of oscillations over a cycle (Magri and Juniper 2013).
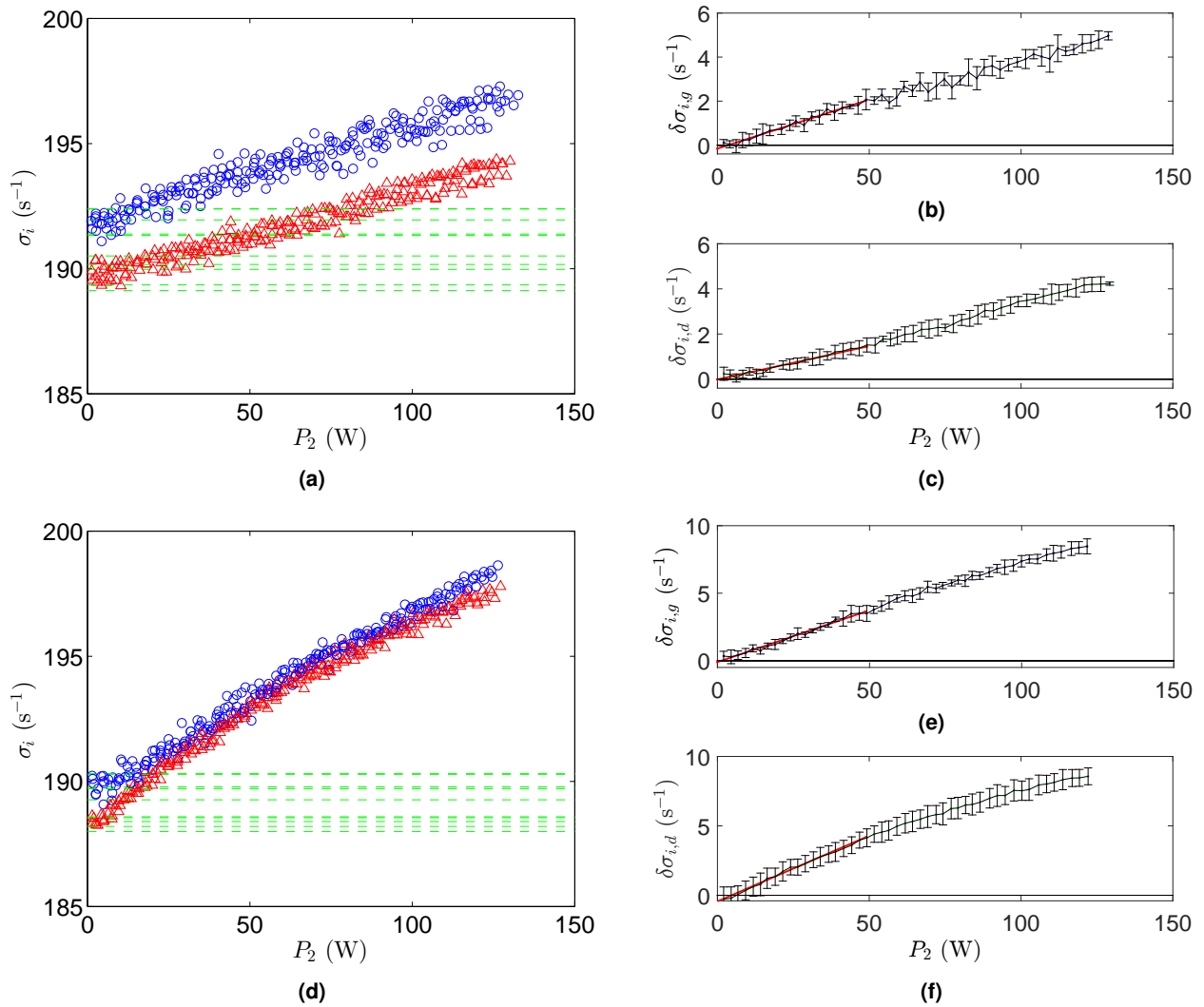
Figure 7. (a) $x_c/L = 0.35$: Frequency during period of growth (blue) and decay (red) of oscillations obtained for a range of secondary heat source powers. All baseline run is shown in the green; (b) $x_c/L = 0.35$: frequency during period of growth with and without the secondary heat source, $\delta\sigma_{r,g}$; (c) $x_c/L = 0.35$: frequency during period of decay with and without the secondary heat source, $\delta\sigma_{r,d}$; (d) $x_c/L = 0.55$: Frequency during period of growth (blue) and decay (red) of oscillations obtained for a range of secondary heat source powers. All baseline run is shown in the green; (e) $x_c/L = 0.55$: frequency during period of growth with and without the secondary heat source, $\delta\sigma_{r,g}$; (f) $x_c/L = 0.55$: frequency during period of decay with and without the secondary heat source, $\delta\sigma_{r,d}$.

We find that when placed at $x_c/L = 0.85$, the secondary heat source is most successful at stabilising the growth of thermoacoustic oscillations. It can be seen in figure 8c that both the shift in linear growth rate and the shift in linear decay rate exhibit the same qualitative trends. However, both sets of data do not overlay perfectly. This is due to changes in the base state of the system. When we measure the growth rates we abruptly increased the power input to the primary heater, which increases the heat transfer from the heater to the mean flow, resulting in a change in base state. Similarly, when we measure the decay rates we abruptly decrease the power input to the primary heater, which decreases the heat transfer from the heater to the mean flow, resulting in a change in base state. This is not accounted for in Magri and Juniper (2013) but will be in future models. Error bars are presented with the experimental data in figure 8c and are discussed in Appendix A.

Shift in frequency during linear growth and decay of oscillations

This section presents the experimental sensitivity analysis results detailing the shift in frequency during periods of linear growth and decay of the thermoacoustic oscillations.

Figure 9a and 9b show $\delta\sigma_{i,g}$ and $\delta\sigma_{i,d}$ for $x_c/L = 0.1$, 0.15, 0.35, 0.45, 0.55, 0.75, and 0.85. These points were chosen so that a clear depiction could be obtained of how the gradient of $\delta\sigma_{i,g}$ and $\delta\sigma_{i,d}$ data varies as the secondary heat source is traversed through a range of axial locations. The coloured patching around the mean $\delta\sigma_{i,g}$ and $\delta\sigma_{i,d}$ has the same meaning as above. Again, at locations $x_c/L = 0.75$ and 0.85 the uncertainty is larger. This is because fewer experimental points are taken at these locations.

The shift in frequency during the periods of linear growth (blue) and decay (red), obtained via the experimental sensitivity analysis, are presented in figure 9c. We compare the experimental results with the predictions of Magri and
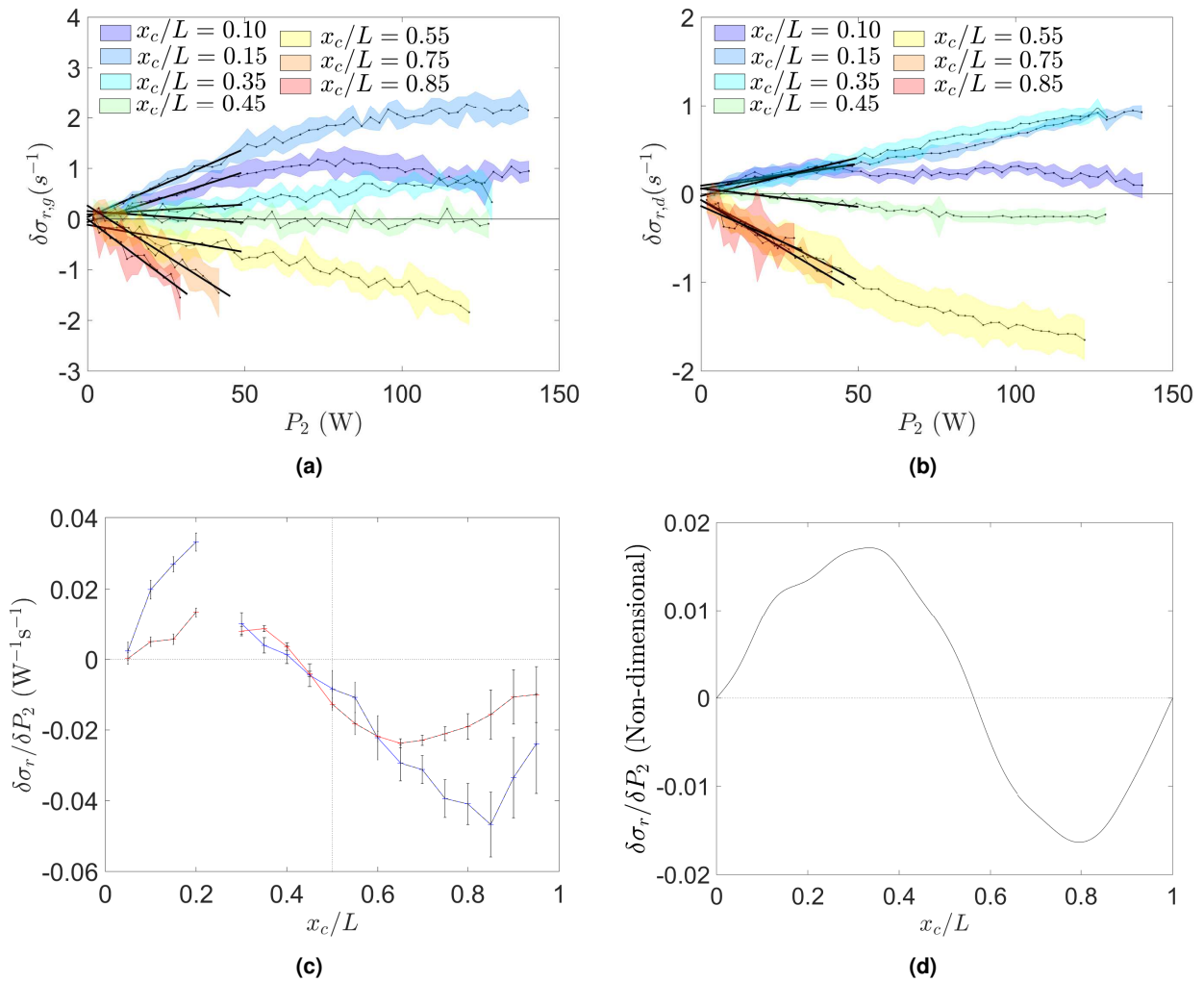
Figure 8. (a) Range of $\delta\sigma_{r,g}$ with the color patch outlining the uncertainty; (b) Range of $\delta\sigma_{r,d}$ with the color patch outlining the uncertainty; (c) The shift in linear growth rate (blue) and linear decay rate (red) due to a secondary heat source; (d) The adjoint-based predicted shift in growth rate due to the heat release (but not the drag) of a secondary heat source (Magri and Juniper 2013).

Juniper (2013) (figure 9d) and find that they do not agree. We find that the experimental results are opposite in sign and shifted on the vertical-axis when compared to the theoretical predictions made by adjoint-based sensitivity analysis.

Magri and Juniper (2013) predict that the introduction of a secondary heat source will have a greater effect on the frequency shift than the growth and decay rate shift. This is manifested in the order of magnitude seen in figure 9d. When we compare the order of magnitude seen in figure 9c with that seen in figure 8c, we find that the secondary heat source does in fact have a greater effect on the shift in frequency during periods of linear growth and decay of oscillations than it does have on the shift in the linear growth and decay rate.

Whilst the experimental sensitivity analysis results for the shift in frequency during periods of growth and decay of oscillations do not match the adjoint-based predictions they are important to present. This discrepancy highlights the limitations of the model in capturing the physics pertaining to the frequency. The physical model of Magri and Juniper (2013) does not adequately describe the mean temperature changes caused by the introduction of a secondary heat source. These experimental results will feed back into

development of the model in order to obtain a more accurate adjoint-based model of the system.

Conclusions and further work

The control of thermoacoustic oscillations is a significant problem in the development of clean and efficient combustion systems. Previous work by Magri and Juniper (2013) has shown that adjoint-based methods are a cheap and efficient computational tool by which optimal control strategies can be developed for the eradication of thermoacoustic oscillations.

We extend the work of Rigas et al. (2016), using a more complex control method, and show that sensitivity analysis can be performed experimentally on a vertical electrically-heated Rijke tube to determine how sensitive the linear growth and decay rates and linear frequencies during periods of growth and decay of thermoacoustic oscillations are to the introduction of a secondary heat source.

Comparing with the results of Magri and Juniper (2013), we find that the qualitative agreement is good for the shift in linear growth and decay rates, but not for the shift in linear frequency during periods of growth and decay.
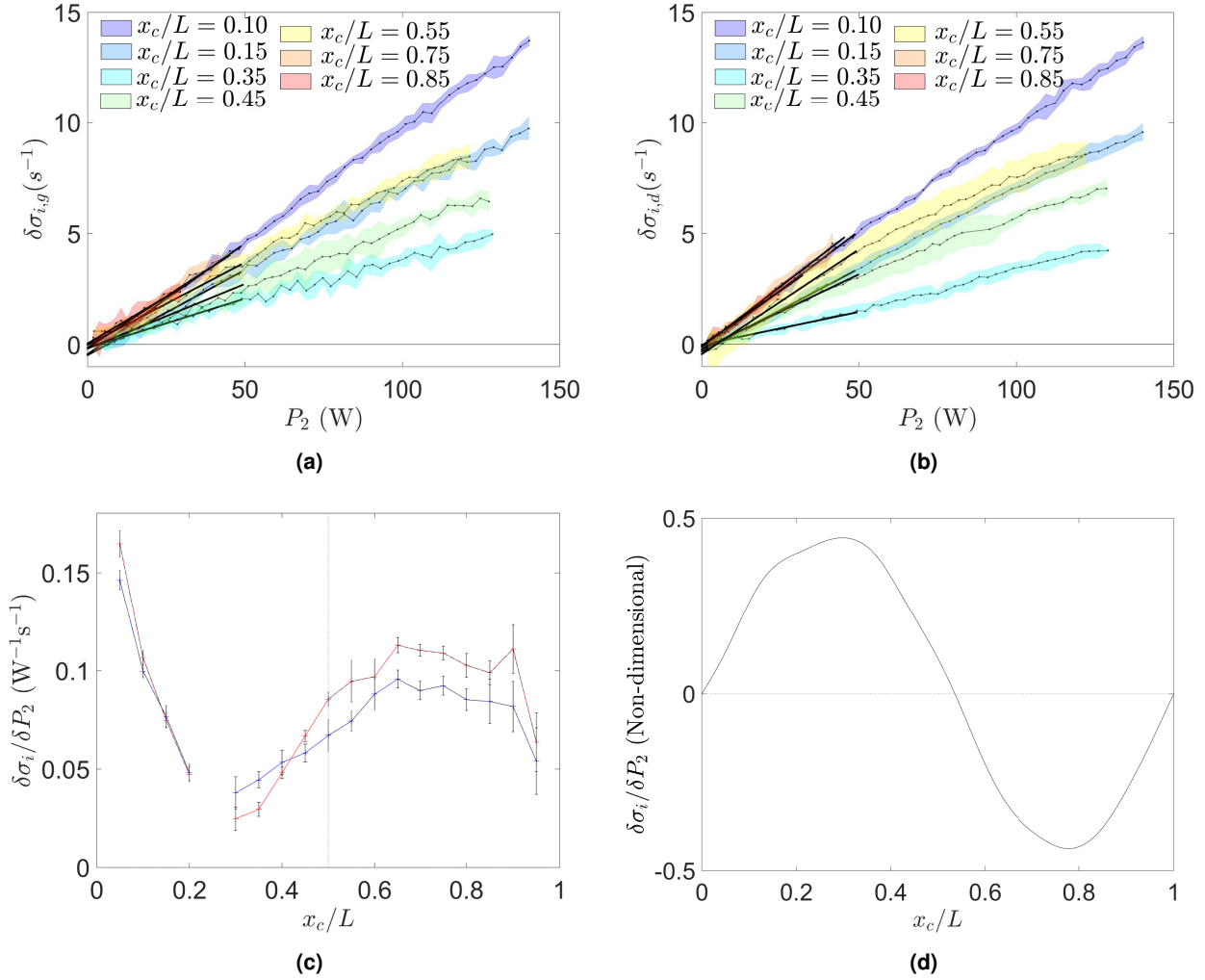
Figure 9. (a) Range of $\delta\sigma_{i,g}$ with the color patch outlining the uncertainty; (b) Range of $\delta\sigma_{i,d}$ with the color patch outlining the uncertainty; (c) The shift in frequency during linear growth (blue) and linear decay (red) due to a secondary heat source; (d) The adjoint-based predicted shift in frequency during period of growth due to a secondary heat source (Magri and Juniper 2013).

These experiments will guide future work in developing a more accurate model of the Rijke tube. Adjoints will be derived for the new model so that all its sensitivities can be calculated and compared with experiments.

Acknowledgements

Appendix A. Uncertainty Analysis

Uncertainties in $\delta\sigma$ measurement

This section presents the method used to determine the uncertainty in the experimental data presented in figures 6b, 6c, 6e, 6f, 7b, 7c, 7e, and 7f. The methodology used is based on pages 101-102 of Taylor (1997). We first calculate the sample standard deviation of each data point using:

$$\hat{\epsilon}_\sigma = \sqrt{\left(\frac{1}{N-1}\right)\sum_{i=1}^{N}(\sigma_i - \bar{\sigma})^2} \tag{3}$$

where N is the number of points obtained, σ_{ii} is the measured growth rate, decay rate, frequency during linear growth, or frequency during linear decay, and $\bar{\sigma}$ is the mean value of σ for a specific secondary heat source power, P_2 (W), and a specific axial location, x_c/L, averaged over the five experimental repetitions. The standard error is then calculated as:

$$\hat{\epsilon}_{error} = \frac{\hat{\epsilon}_\sigma}{\sqrt{N}} \tag{4}$$

The uncertainty were presented as $2\hat{\epsilon}_{error}$ to allow for a 95% confidence interval. The error bars were plotted against the mean P_2 (W) and the mean σ.

Uncertainties in $\delta\sigma/\delta P_2$ measurement

This section presents the method used to determine the uncertainty in the experimental data presented in figure 8c and 9c. The methodology used is based on pages 187-188 of Taylor (1997). We calculate the uncertainty of the fitting of the $\delta\sigma$ data so that we can determine the uncertainty in the shift in growth and decay rates and the frequency shift during the growth and decay of oscillation (figure 8c and 9c). The fitting of the $\delta\sigma$ data is not forced to go through the origin,

thus the line being fitted is of the form $\delta\sigma = BP_2 + A$. We first calculate the uncertainty in the measurements of y:

$$\varepsilon_y = \sqrt{\left(\frac{1}{N-2}\right)\sum_{j=1}^{N}[\delta\sigma_j - A - BP_{2,j}]^2}, \qquad (5)$$

where N is the number of points obtained, $\delta\sigma_j$ is the measured growth rate, decay rate, frequency during linear growth, or frequency during linear decay, A and B are constants obtained from the least-squares regression fitting for each axial location, x_c/L, and $P_{2,j}$ are the secondary heat source powers examined. The least-squares regression fitting is between the first σ point and the final σ point which corresponds to a secondary heat source power less than 50 W, i.e. $P_2 < 50$W. The above result is then used to determine the uncertainty in the measurement of the sensitivity, $\delta\sigma/\delta P_2$. This is calculated using:

$$\varepsilon_B = \varepsilon_y \sqrt{\frac{N}{\triangle}} \qquad (6)$$

where

$$\triangle = N\sum_{j=1}^{N}[P_{2,j}]^2 - \left(\sum_{j=1}^{N}[P_{2,j}]\right)^2 \qquad (7)$$

We are only interested in the uncertainty in the constant B. This is the gradient of the least-squares regression fitting which we present in figure 8c and 9c. The uncertainty is presented with a 95% confidence interval, i.e. the uncertainty is presented as $2\varepsilon_B$ (Taylor 1997).

References

Candel, S. M. (2002). Combustion dynamics and control: Progress and challenges. *Proc. Combust. Inst.*, 29:1–28.

Culick, F. E. C. (1988). Combustion Instabilities in Liquid-Fuelled Propulsion Systems. Technical Report 430.

Dowling, A. P. and Morgans, A. S. (2005). Feedback Control of Combustion Oscillations. *Annu. Rev. Fluid Mech.*, 37(1):151–182.

Heckl, M. A. (1988). Active control of the noise from a rijke tube. *J. Sound Vib.*, 124(1):117–133.

Katto, Y. and Sajiki, A. (1977). Onset of oscillation of a gas-column in a tube due to the existence of heat-conduction field: a problem of generating mechanical energy from heat. *Bulletin of JSME*, 20(147):1161–1168.

Lieuwen, T. and Zinn, B. T. (1998). The role of equivalence ratio oscillations in driving combustion instabilities in low NOx gas turbines. *Symp. (Intl.) on Comb.*, 27(2):1809–1816.

Lieuwen, T. C. and Yang, V. (2005). Combustion instabilities in gas turbine engines: operational experience, fundamental mechanisms and modeling. *Prog. in Astro. and Aero.*

Lighthill, M. J. (1954). The Response of Laminar Skin Friction and Heat Transfer to Fluctuations in the Stream Velocity The response of laminar skin friction and heat transfer to fluctuations in the stream velocity. *Proc. of the Royal Society of London. Series A, Mathematical and Physical Sciences*, 224(1156):1–23.

Luchini, P. and Bottaro, A. (2014). Adjoint Equations in Stability Analysis. *Annu. Rev. Fluid Mech.*, 46(1):493–517.

Magri, L. and Juniper, M. P. (2013). Sensitivity analysis of a time-delayed thermo-acoustic system via an adjoint-based approach. *J. Fluid Mech.*, 719:183–202.

Magri, L. and Juniper, M. P. (2014a). Adjoint-based linear analysis in reduced-order thermo-acoustic models. *Int. J. Spray Combust. Dyn.*, 6(3):225–246.

Magri, L. and Juniper, M. P. (2014b). Global modes, receptivity, and sensitivity analysis of diffusion flames coupled with duct acoustics. *J. Fluid Mech.*, 752:237–265.

McManus, K. R., Poinsot, T., and Candel, S. M. (1993). A review of active control of combustion instabilities. *Prog. Energy Combust. Sci.*, 19:1–29.

Raun, R. L., Beckstead, M. W., Finlinson, J. C., and Brooks, K. P. (1993). A Review of Rijke Tubes, Rijke Burners and Related Devices. *Prog. Energ. Combust.*, 19:313–364.

Rayleigh, J. W. S. (1878). The Explanation of Certain Acoustical Phenomena. *Nature (London)*, 18:319–321.

Rigas, G., Jamieson, N. P., Li, L. K. B., and Juniper, M. P. (2016). Experimental sensitivity analysis and control of thermoacoustic systems. *J. Fluid Mech.*, 787(R1):1–11.

Rijke, P. L. (1859). On the vibration of the air in a tube open at both ends. *Phil. Mag.*, 17:419–422.

Saito, T. (1965). Vibrations of Air-Columns Excited by Heat Supply. *The Japan Society of Mechanical Engineers*, 8(32).

Schmid, P. J. and Brandt, L. (2014). Analysis of Fluid Systems: Stability, Receptivity, Sensitivity. *App. Mech. Rev.*, 66(2):1–21.

Schumm, M., Berger, E., and Monkewitz, P. A. (1994). Self-excited oscillations in the wake of two-dimensional bluff bodies and their control. *J Fluid Mech.*, 271:17–53.

Sipp, D., Marquet, O., Meliga, P., and Barbagallo, A. (2010). Dynamics and control of global instabilities in open-flows: a linearized approach. *Appl. Mech. Rev.*, 63(3):030801.

Sreenivasan, K., Raghu, S., and Chu, B. (1985). The control of pressure oscillations in combustion and fluid dynamical systems. In *1985 AIAA Shear Flow Control Conf.*

Taylor, J. R. (1997). *An Introduction to Error Analysis: The Study of Uncertainties in Physical Measurements (Second Edition)*. University Science Books, Sausalito, California, USA.

Zhang, Z., Zhao, D., Han, N., Wang, S., and Li, J. (2015). Control of combustion instability with a tunable Helmholtz resonator. *Aerosp. Sci. Technol.*, 41:55–62.

Zhao, D., Ji, C., Li, X., and Li, S. (2015). Mitigation of premixed flame-sustained thermoacoustic oscillations using an electrical heater. *Int. J. Heat Mass Tran.*, 86:309–318.